Journal of Molecular Catalysis A: Chemical 339 (2011) 8–16

Contents lists available at ScienceDirect

Journal of Molecular Catalysis A: Chemical

journal homepage: www.elsevier.com/locate/molcata

Research paper

Effect of the chromium precursor nature on the physicochemical and catalytic properties of Cr–ZSM-5 catalysts: Application to the ammoxidation of ethylene

F. Ayari[a,*], M. Mhamdi[a], D.P. Debecker[b], E.M. Gaigneaux[b], J. Alvarez-Rodriguez[c], A. Guerrero-Ruiz[c], G. Delahay[d], A. Ghorbel[a]

[a] Laboratoire de Chimie des Matériaux et Catalyse, Département de Chimie, Faculté des Sciences de Tunis, Campus Universitaire Tunis ElManar, 2092 Tunis, Tunisia
[b] Université catholique de Louvain, Institue of Condensed Matter and Nanosciences (IMCN) – Division: Molecules, Solids and Reactivity (MOST), Croix du Sud 2/17, B-1348 Louvain-la-Neuve, Belgium
[c] Unidad Asociada Group for Desig. and Appl. of Heter. Catal. UNED-ICP (CSIC), Dpto. Inorganic and Technical Chemistry, Faculty of Sciences, UNED, 28040 Madrid, Spain
[d] Institut Charles Gerhardt Montpellier, UMR 5253, CNRS-UM2-ENSCM-UM1, Eq. "Matériaux Avancés pour la Catalyse et la Santé", ENSCM (MACS - Site la Galéra), 8, rue Ecole Normale, 34296 Montpellier Cedex 5, France

ARTICLE INFO

Article history:
Received 18 November 2010
Received in revised form 15 February 2011
Accepted 18 February 2011
Available online 26 February 2011

Keywords:
Cr–ZSM-5
Solid-state exchange
Ammoxidation
Acetonitrile
XPS spectroscopy

ABSTRACT

The catalytic performance of Cr–ZSM-5 catalysts prepared by solid-state reaction from different chromium salts (acetate, chloride, nitrate and ammonium dichromate) was evaluated in the selective ammoxidation of ethylene to produce acetonitrile. Cr–ZSM-5 catalyst characterization by chemical analysis, XRD, FTIR, N_2 physisorption, ^{27}Al MAS NMR, TEM/EDX, UV–visible DRS, XPS, Raman and DRIFT spectroscopies and H_2-TPR is reported. From textural analysis, it is obvious, after chromium exchange, that a decrease of S_{BET} and of porous volume is observed. On the other hand, FTIR, XRD and ^{27}Al MAS NMR results show that there is no collapse of the parent zeolite during thermal treatment. From H_2-TPR, DRS, Raman and XPS spectroscopies, it is concluded that Cr ions and Cr(III) oxide coexist. TEM/EDX results confirmed that chromium oxide species are either heterogeneously or homogeneously dispersed on the support, depending on the nature of the precursor. DRIFT showed that chromium exchange leads strictly to the consumption of Si–O$^+$H–Al groups. The catalyst prepared from chromium chloride showed higher activity and selectivity towards acetonitrile, being this catalytic modification probably due to the differentiated nature of chromium species formed using this precursor. A similarity with Fe–ZSM-5 system is underlined. In fact, higher oxidation states of chromium species are required for ethylene ammoxidation, while Cr_2O_3 clusters seem to enhance the hydrocarbon oxidation.

1. Introduction

One of the great fields of heterogeneous catalysis is the conversion of light hydrocarbons into more useful chemicals such as nitrile compounds. In particular, selective ammoxidation of ethylene is of prime practical significance [1] as it could be an additional source of acetonitrile. The industrial production of this chemical compound implies the use of hazardous, high cost and low-selectivity processes. As an alternative, firstly, Li and Armor [2] and Wichterlová et al. [3], and more recently Ghorbel et al. [4,5], have reported that ethylene can be efficiently converted to acetonitrile in the presence of ammonia and oxygen using cobalt exchanged zeolites or with alumina supported Co or Cr catalysts.

Chromium exchanged zeolites offer high catalytic activity for a wide variety of important reactions such as ethylene polymerization [6], oxidation of hydrocarbons [7], cracking of cumene [8], disproportionation of n-heptane [8], isomerization of methyl-3-pentane [8] and thermolysis of H_2O [9]. More recently, we have reported [10] that ethylene can be efficiently converted to acetonitrile over Cr–ZSM-5 catalysts.

Due to the catalytic properties of chromium containing catalysts, several attempts have been carried out in order to introduce Cr cations into molecular sieves. The most common strategies being hydrothermal synthesis [11,12], aqueous ion exchange (AE) [13–15] and solid state ion exchange (SSE) [16]. Solid-state ion exchange occurs by the diffusion of metal ions into a zeolite via the heating of a mixture of two finely ground powders: the zeolite and the chromium salt [17,18]. When compared to AE, SE has several potential advantages. Firstly, it is carried out at atmospheric pressure and avoids the handling of large volumes of solution. Secondly, AE leads to a waste in salt due to the fraction of ions that have not been exchanged, whereas all the salt is retained by the zeolite in solid-state synthesis, even if introduced in over-stoichiometric ratios. Thirdly, with solid-state reaction, parameters difficult to control such as pH, cation size and solvatation phenomena, are avoided. Several factors influence the catalytic activity of chromium

* Corresponding author. Tel.: +216 98691919; fax: +216 71885008.
E-mail address: lcmc_fa@yahoo.fr (F. Ayari).

1381-1169/$ – see front matter © 2011 Elsevier B.V. All rights reserved.
doi:10.1016/j.molcata.2011.02.012

catalysts such as the oxidation state, the structure (amorphous or crystalline, mono/di-chromate or polychromates, etc.) and the interaction of the chromium species with the support, which essentially depend on the catalyst preparation method. These factors are principally governed by different parameters such as the metal loading, the support characteristics, and the nature of the post-treatment (calcination, reduction, etc.). Whatever the preparation method, it is believed that different oxidation states of chromium, in particular, Cr(VI), Cr(V), Cr(III) and Cr(II), can be stabilized inside the zeolite structures, each with their specific coordination geometry [19]. For example, after AE, $Cr(H_2O)_6^{3+}$ or $Cr(H_2O)_6^{2+}$ ions are present in the cavities and/or channels of zeolite and these ions migrate onto the surface after dehydration. Furthermore, SE followed by calcination results in the migration of Cr into the zeolite channels and cavities, where it is present at higher oxidation states. Reduction treatment leads to the formation of Cr(V), Cr(III), and Cr(II), although Cr(0) is also claimed [20]. Pearce and Mortier [21] demonstrated by X-ray diffraction (XRD) that Cr(III) ions are located at the three-coordinated site (I′) in dehydrated Faujasite structures, at least at relatively high Cr loadings.

The nature of metal precursor is another parameter, which can affect the predominance of chromium species in zeolite. In the case of SE, the exchange process initially takes place at the solid–solid interface between the precursor salt and zeolite grains, and the success of the exchange depends on the type of interactions developed. Overstoichiometric exchanges can be expected from SE while they cannot be obtained in solution. Nevertheless, the extent of the exchange in the narrowest sense (i.e., leading to the cations in exchanged positions) can be higher or lower depending on the formation of extraframework phases at the expense of the migration of ions into the zeolite channels [22,23], resulting in a different speciation.

The aim of this work is to study the effect of the nature of the precursor on the physicochemical properties of Cr–ZSM-5 catalysts and their catalytic performance in the ammoxidation of ethylene into acetonitrile.

2. Experimental

2.1. Catalyst preparation

Solid-state exchange reaction was performed as follows: an appropriate amount of H–ZSM-5 support (Zeolyst, Si/Al = 15) was mixed with chromium salts (Cr acetate (Strem Chemical), Cr chloride (Prolabo), Cr nitrate (99%, Acros Organics) and ammonium dichromate (99%, Merck)) in the desired molar ratio Cr/Al = 1. The finely grounded powders obtained by mechanical mixture were heated for 12 h (heating rate 2 °C/min) at 500 °C in helium. Catalysts were labelled Cr–P, where P refers to the chromium precursor. CrO_3–ZSM-5 and Cr_2O_3–ZSM-5 catalysts were prepared by a simple mechanical mixture of CrO_3 (Merck 99%) and Cr_2O_3 (Aldrich 99.9%) with H–ZSM-5, followed by helium treatment for 1 h at 500 °C (heating rate 5 °C/min) to serve as a reference in catalytic tests.

2.2. Catalyst characterization

The chemical element (Cr, Si, Al) content of catalysts was determined by ICP at the Vernaison Center of the CNRS (France).

N_2 adsorption–desorption isotherms were determined at 77 K with an automatic ASAP 2000 apparatus from Micromeritics after pretreatment under vacuum at 200 °C for 5 h. Specific surface area was determined by BET method, microporous volume by *t*-plot method and porous volume was taken as the volume adsorbed at $P/P^\circ = 0.98$.

XRD measurements were performed in an X'Pert Pro X-ray diffractometer from PANalytical with CuKα radiation ($\lambda = 1.54060$ Å), with generator setting of 40 kV and 40 mA, a scanning speed of 0.05°/min, and scanning region of 20–70°. The diffractometer was operated at 1.0° diverging and 0.1° receiving slits and a continuous intensity trace was recorded as function of 2θ. Structural data identification was performed using EVE software.

FTIR spectra were recorded on a Perkin Elmer (Spectrum BX) spectrometer in the wavenumber range 4000–400 cm^{-1} at a spectral resolution of 4 cm^{-1} and accumulating 100 scans.

X-ray spectroscopy studies (EDX) were realized using a Quanta 200 FEG Electron Microscopy spectrometer calibrated using Co as optimization element. All results were obtained at High Vacuum mode.

TEM studies were carried out in a JEOL JEM-2000 FX microscope at 200 kV. The samples were prepared by grinding and ultrasonic dispersal into an acetone solution, placed on a TEM copper grid, and evaporated.

^{27}Al MAS NMR spectra were recorded at 78.20609 MHz on a Bruker WB spectrometer using $AlClO_3 \cdot 6H_2O$ as reference. An overall 4096 free induction decays were accumulated. The excitation pulse and recycle time were 6 μs and 0.06 s, respectively.

DRS spectra were recorded in the wavelength range 900–200 nm on a Perkin Elmer Lambda 45 spectrophotometer equipped with a diffuse reflectance attachment. Parent zeolite was the reference material for all catalysts. The DR spectra were converted to the Kubelka-Munk function in order to convert reflectance data into pseudo-absorbance.

Raman measurements were carried out on a confocal Thermo Scientific DXR Raman Microscopy system using the visible line at 532 nm. The maximum incident power at the sample was approximately 10 mW.

XPS analyses were performed on a SSX 100/206 photoelectron spectrometer from Surface Science Instruments (USA) equipped with a monochromatized micro focused Al X-ray source (1486.6 eV, powered at 20 mA and 10 kV). Before analysis, the powders were pressed in small stainless steel troughs of 4 mm diameter and were placed on an aluminum conductive carousel. The pressure in the analysis chamber was around 10^{-6} Pa. The angle between the surface normal and the axis of the analyser lens was 55°. The analysed area was approximately 1.4 mm^2 and the pass energy was set at 150 eV. The C-(C, H) component of the C 1s peak of carbon has been fixed to 284.8 eV to set the binding energy scale. Data treatment was performed with the CasaXPS program (Casa Software Ltd., UK). Some Cr 2p peaks were decomposed in several doublets taking into account that the theoretical distance between Cr $2p_{1/2}$ and Cr $2p_{3/2}$ peaks is 9.8 eV and the area ratio is 2/3. Molar fractions were calculated using peak areas normalised on the basis of acquisition parameters and sensitivity factors provided by the manufacturer.

H_2-TPR analysis was performed with a Micromeritics Autochem 2910 Analyser, in a Pyrex U-tube reactor and an on-line thermal conductivity detector (TCD). The catalyst (70 mg) was dried at 500 °C for 1 h in air and reduced from 50 to 1000 °C (15 °C/min) with 3% H_2/Ar flow.

DRIFT spectra were recorded on a Bruker IFS 55 spectrometer equipped with a Thermo Spectra Tech reacting cell at a spectral resolution of 4 cm^{-1} and accumulating 200 scans. Samples were treated in situ at 500 °C with helium (ramp: 5 °C/min, flow: 30 cm^3/min).

Ammoxidation of ethylene was studied with 100 mg of catalyst between 400 and 500 °C using a tubular glass reactor. In all cases, the inlet reactant composition was 10% O_2 (Air Liquide 99.995%), 10% C_2H_4 (Air Liquide 99.995%), 10% NH_3 (Air Liquide 99.96%). The total flow rate was then maintained at 100 cm^3/min by balancing with helium (Air Liquide 99.998%) flow rate. Prior to the

catalytic test, samples were activated in situ under helium flow (70 cm^3/min) up to 500 °C. The analysis of the outlet flow was recorded on-line by two chromatographic units, one operated with a flame ionization detector, while the other was equipped with a thermal conductivity detector. The conversion, selectivity and activity are defined as follow:

Conversion of C_2H_4:

$$X = \frac{\sum_i y_i n_i}{y_E n_E + \sum_i y_i n_i}$$

Selectivity of product P_i:

$$S_i = \frac{y_i n_i}{\sum_i y_i n_i}$$

Activity of product P_i:

$$A_i = \frac{n_a \times 190.97}{m_{catalyst}}$$

where y_i and y_E are the mole fractions of product P_i (CH_3CN) and C_2H_4, respectively; n_i and n_E are the number of carbon atoms in each molecule of product P_i and C_2H_4, respectively, and n_a and $m_{catalyst}$ are the mole number of produced acetonitrile and catalyst weight, respectively.

3. Results

3.1. Chemical analysis

Table 1 collects the elemental analysis results of the parent zeolite and Cr–P solids. The values obtained for Si and Al fit with the data provided by the zeolite manufacturer. On the other hand, the chromium content ultimately retained by the zeolite during solid-state exchange varies and depends on the nature of the metal precursor. For all catalysts, Cr/Al molar ratios are close to the nominal value except the Cr–Cl catalyst, which exhibits the lowest Cr/Al ratio. Besides elemental analysis, ion exchange degree is presented in Table 1. 100% ion exchange degree is calculated on the basis of 3 × Cr/Al (mol/mol) in the case of Cr(III) salts and 6 × Cr/Al (mol/mol) for ammonium dichromate. Cr–A, Cr–N and Cr–D catalysts contain much more metal ion than required for 100% ion-exchange. These samples are regarded as 'over-exchanged' materials contrarily to Cr–Cl catalyst, which exhibits an 80% exchange degree. In ZSM5, the positions of tetrahedrally coordinated Al^{3+} ions are spatially very separated and therefore, bare Cr^{3+} or Cr^{6+} cations cannot exist since it would be necessary to have 3 or 6 aluminum neighbors. In fact, similarly to Fe–ZSM-5 system [24], it is possible to have the presence of chromium (hydr)oxocation species like $[OH–Cr–O–Cr–OH]^{2+}$ species, for example.

3.2. Textural properties

The adsorption–desorption isotherms of prepared materials are presented in Fig. 1. Catalysts as well as the zeolite support exhibit a type I isotherm according to the BDDT classification [25] with a plateau at higher relative pressures evidencing the microporous nature of the materials with a limited mesoporosity. The textural properties obtained from the N_2-adsorption/desorption isotherms of the zeolite samples are summarized in Table 2.

The obtained data revealed that the introduction of chromium is accompanied by a decrease in the BET surface area due to a decrease of the microporous volume. This effect may be attributed to the presence of oxide aggregates and/or extra-framework aluminum species inside the zeolite pores and channels.

Table 1
Chemical analysis results.

Sample	Cr (wt.%)	Al (wt.%)	Si/Al (mol/mol)	Cr/Al (mol/mol)	Ion exchange degree (%)
H–ZSM-5	–	2.6	15.1	–	–
Cr–A	5.1	2.2	15.1	1.20	296
Cr–Cl	1.4	2.2	15.0	0.33	80
Cr–N	4.5	2.2	15.4	1.06	257
Cr–D	3.9	2.2	15.3	0.92	458

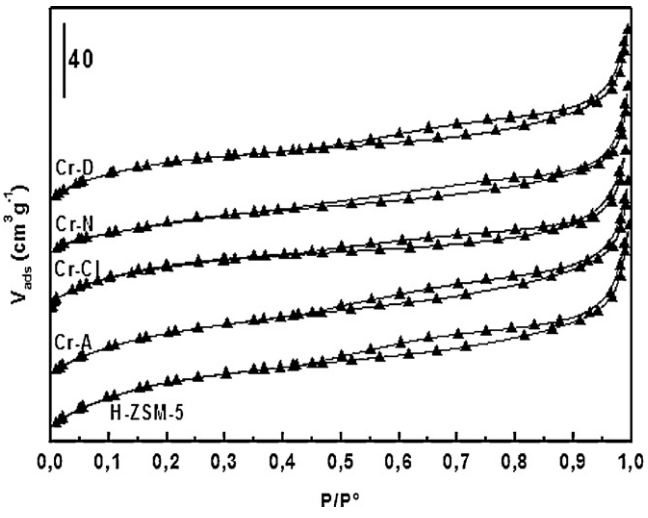

Fig. 1. N_2 adsorption–desorption isotherms of the zeolite support and catalysts.

Table 2
BET surface area and porosity measurements.

Sample	S_{BET} (m^2 g^{-1})	S_μ (m^2 g^{-1})	V_μ (cm^3 g^{-1})	V_p (cm^3 g^{-1})
H–ZSM-5	340	198	0.118	0.261
Cr–A	319	185	0.099	0.238
Cr–Cl	304	186	0.110	0.228
Cr–N	248	161	0.092	0.198
Cr–D	291	213	0.121	0.225

3.3. TEM–EDX study

EDX analysis was performed in four different points at the catalyst surface. Results are compiled in Table 3. Data show that all the zeolite grains do not support a constant quantity of chromium. In fact, heterogeneity of Cr deposit (high discrepancies in the Cr/Al ratio) is marked in the case for Cr–Cl and Cr–N catalysts. Het-

Table 3
EDX results.

Cata.	Al	Si	Cr	Cr (wt.%)	Cr/Al	Si/Al
Cr–A	1.48	23.04	1.49	3.97	1	15.56
	1.31	24.93	1.70	4.46	1.29	19.03
	1.49	27.02	1.84	4.76	1.23	18.13
	1.75	31.97	2.20	5.49	1.05	18.26
Cr–N	0.63	8.43	20	43	31.74	13.38
	1.84	34.44	0.1	0.25	0.05	18.71
	1.46	23.98	6.06	14.85	4.15	16.42
	1.47	24.72	0.08	0.21	0.05	16.81
Cr–Cl	1.82	31.69	2.05	5.14	1.12	17.41
	1.52	26.40	0.95	2.50	0.62	17.36
	1.50	27.24	2.39	6.18	1.59	18.16
	1.54	21.42	2.32	8.36	1.50	16.73
Cr–D	2.12	37.15	0.49	1.21	0.23	17.52
	2.05	36.72	0.67	1.18	0.32	17.91
	1.86	31.39	0.61	1.56	1.86	16.87
	1.95	24.72	1.44	3.61	0.73	12.67

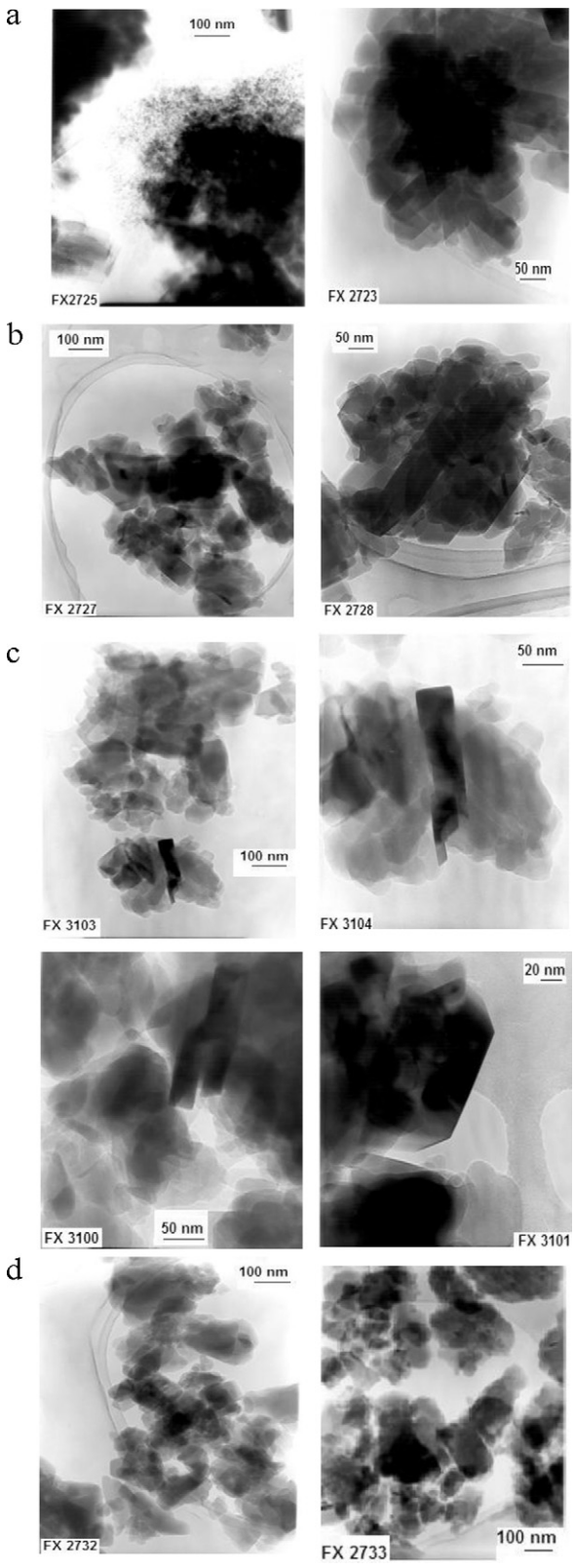

Fig. 2. TEM images of: (a) Cr–A; (b) Cr–N; (c) Cr–Cl and (d) Cr–D.

erogeneities in aluminum distribution have also been detected for all catalysts, as has already been reported for ZSM-5 crystals [26].

TEM images of Cr–A catalyst are shown in Fig. 2a. This sample consists of spherical chromium oxide particles of a significant size

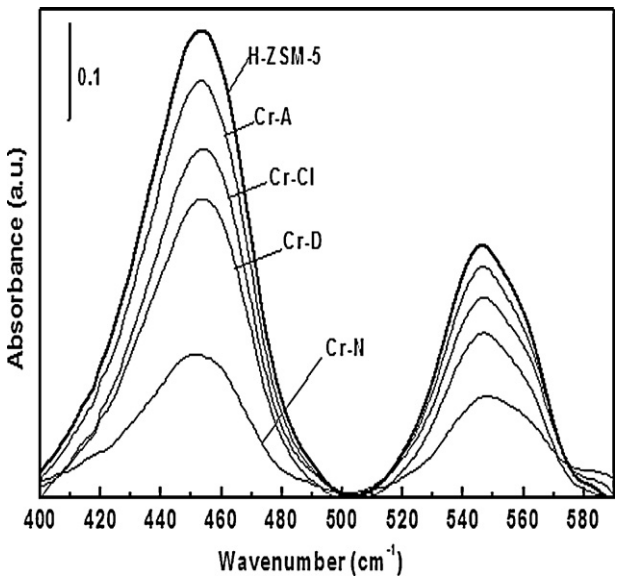

Fig. 3. FTIR plots of the support and catalysts.

as well as large sized cubic and rhombohedric siliceous particles. The dispersion of chromium is homogenous ($wt_{Cr} \sim 5\%$) as demonstrated by EDX results. For Cr–N catalyst (Fig. 2b), the chromium is heterogeneously dispersed but no aggregate particles are detected at the surface. For Cr–Cl catalyst (Fig. 2c), TEM images reveal the presence of half built polygonal particles, which consist of chromia, coexisting between "apparent spongy" silica particles (see FX3100). Chromium is heterogeneously dispersed as shown in Table 3. On the other hand, Cr–D catalyst (Fig. 2d) exhibits measles or strawberry shaped particles. Chromium is homogeneously dispersed.

3.4. Structural properties

Crystallinity loss was evaluated by comparing the area ratio of 450 and 550 cm^{-1} infrared bands with that of the parent ZSM-5 [27,28], which was considered to be 100% crystalline. The band situated at 450 cm^{-1} corresponds to the internal vibrations of primary structural units, while the band at 550 cm^{-1} is attributed to the vibration of larger parts of the structure. This band is so-called external [29]. FTIR plots are presented in Fig. 3. The determination and the comparison of different area ratios proved that there was no significant damage of H–ZSM-5 zeolite during thermal treatment. In fact, the non-considerable crystallinity reduction is of 16, 8, 15 and 2%, respectively for Cr–A, Cr–Cl, Cr–N and Cr–D catalysts.

XRD patterns of materials are shown in Fig. 4. Most catalysts exhibit diffraction peaks that are typical of crystalline ZSM-5 (Fig. 4a). This indicates that chromium species deposited during the preparation are either well dispersed over the zeolite in the form of particles of less than 4 nm in size or in the form of small metal oxide clusters that do not show X-ray diffraction. Nevertheless, Cr–N catalyst clearly reveals additional XRD lines at $2\theta = 34^\circ$, 36°, 42°, 51°, and 56° attributable to α-Cr_2O_3 (identification using EVE® software), which can be formed and aggregated during the thermal decomposition of nitrate ions.

^{27}Al MAS NMR spectra of both zeolite catalysts and support are shown in Fig. 5. There is a strong signal at the chemical shift of around $\delta = 60$ ppm which corresponds to tetrahedrally coordinated aluminum in the framework [30]. The weak signal observed ~0 ppm is attributed to octahedral aluminum atoms extracted from the framework [30].

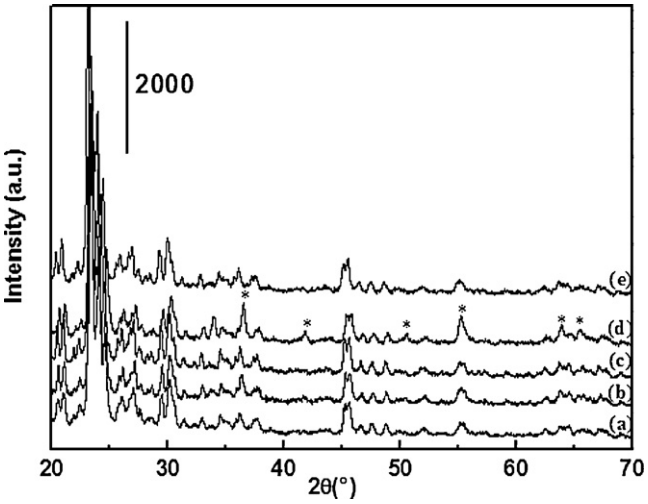

Fig. 4. XRD patterns of (a) H–ZSM-5; (b) Cr–A; (c) Cr–Cl; (d) Cr–N and (e) Cr–D. (*): Cr_2O_3.

^{27}Al MAS spectra show that there is no significant damage of the zeolite structure during solid-state reaction. According to the NMR spectrum of the zeolite support, the octahedral aluminum peak intensity does not exhibit any change after chromium loading.

3.5. DRS, Raman and XPS spectroscopy

UV–visible DRS spectra of catalysts are illustrated in Fig. 6. Spectra are dominated by different types of DRS bands: the support band situated at 203–215 nm, two charge transfer (CT) bands situated at 244–257 and 361–366 nm and d–d transition band situated at 573–612 nm [31–33].

CT bands are typical for $O^{2-} \rightarrow Cr^{6+}$ CT of metallochromates, while d–d transition band is assigned to Cr^{3+} ions.

It has been reported [34] that the band situated at around 450 nm is characteristic of Cr(VI) polychromates.

Raman spectra of mechanical mixtures of CrO_3–ZSM-5 and Cr_2O_3–ZSM-5 (5 wt.%) and catalysts are presented in Figs. 7 and 8, respectively. H–ZSM-5 zeolite does not show any Raman feature in the 200-1100 cm^{-1} region and, therefore, all the observed Raman bands are assigned to chromium species vibrations.

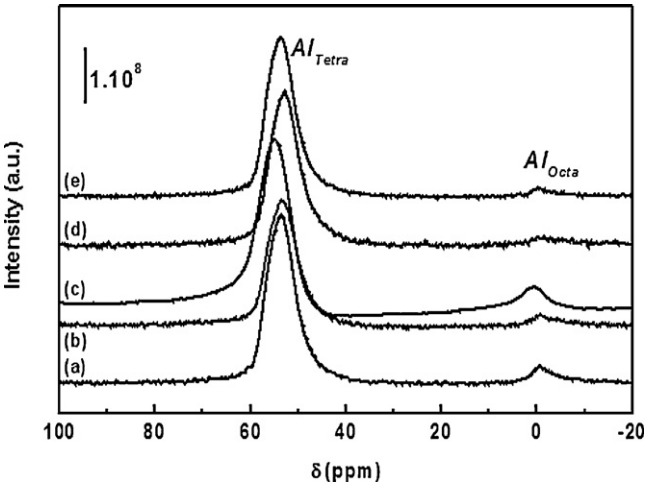

Fig. 5. ^{27}Al MAS NMR spectra of both zeolite catalysts and support: (a) H–ZSM-5; (b) Cr–A; (c) Cr–Cl; (d) Cr–N and (e) Cr–D.

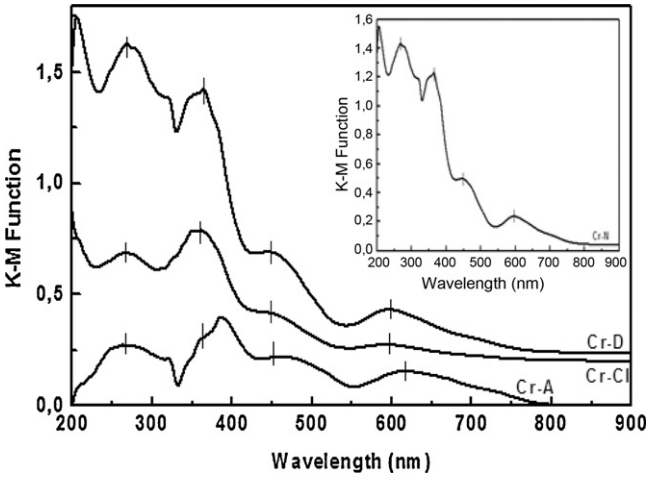

Fig. 6. DRS spectra of catalysts.

It is generally accepted that there are three kinds of chromium species, namely isolated monochromate, polychromate, and crystal Cr_2O_3 in supported chromium solids. The Raman bands at 360 and 860 cm^{-1} are attributable to isolated monochromate species [35–38], the ones at 750–1010 cm^{-1} indicate the presence of Cr^{6+} species in the form of polychromates with different degrees of polymerization [35,36,39–44], whereas those at 550–640 cm^{-1} to crystal Cr_2O_3 [40,45].

Raman spectrum of CrO_3–ZSM-5 solid exhibits two bands at 374 and 1000 cm^{-1} attributed to the symmetric vibration of monochromate and to the Cr–O vibrations of polychromates, respectively. Raman spectrum of Cr_2O_3–ZSM-5 solid exhibits a unique band situated at 553 cm^{-1} attributed to Cr^{3+} species.

For Cr–Cl and Cr–D catalysts, bands at 827–887 and 369–375 cm^{-1} are ascribed to the symmetric stretching and bending modes for an isolated tetrahedral surface of Cr(VI) oxide species, respectively [44–47].

As mentioned previously, the distance between Al atoms in the ZSM-5 framework does not consider the possibility to have bare chromium cations at the exchange sites. Like for Fe–ZSM-5 systems [24], it is rather (hydr)oxo chromium species whose the structure is octahedral.

The weak Raman band situated at 548–551 cm^{-1} is attributed to octahedral Cr^{3+} [44].

In addition, Cr–D catalyst spectra exhibits Raman band at 1010 cm^{-1}, which is attributed to Cr–O vibration of polychromates [44].

Raman spectrum of Cr–A catalyst is not very well resolved. It is dominated by two bands situated at 295 and 550 cm^{-1}, which indicate the presence of both monochromates and octahedral Cr^{3+} species.

Cr–N catalyst Raman spectrum exhibits bands at 302, 343, 370 and 1007 cm^{-1} attributed to monochromates and polychromates species. The bands situated at 541and 597 cm^{-1} indicate the presence of crystalline Cr_2O_3 [45,46], in agreement with XRD results.

It seems that the majority of chromium species are hexacoordinated in the form of mono/poly-chromates and (hydr) oxocationic Cr species in the case of Cr–Cl and Cr–D catalysts. Nevertheless, Cr(III) species are either spread in an amorphous or microcrystalline (XRD undetectable) state, or as crystallized in the case of the Cr–N catalyst.

The oxidation states of Cr species were investigated using XPS. Spectral details are given in Table 4.

XPS results suggest the presence of two distinct Cr species on the surface of catalysts: Cr^{6+} (peaks at 580 and 589.8 eV) and Cr^{3+} (ones

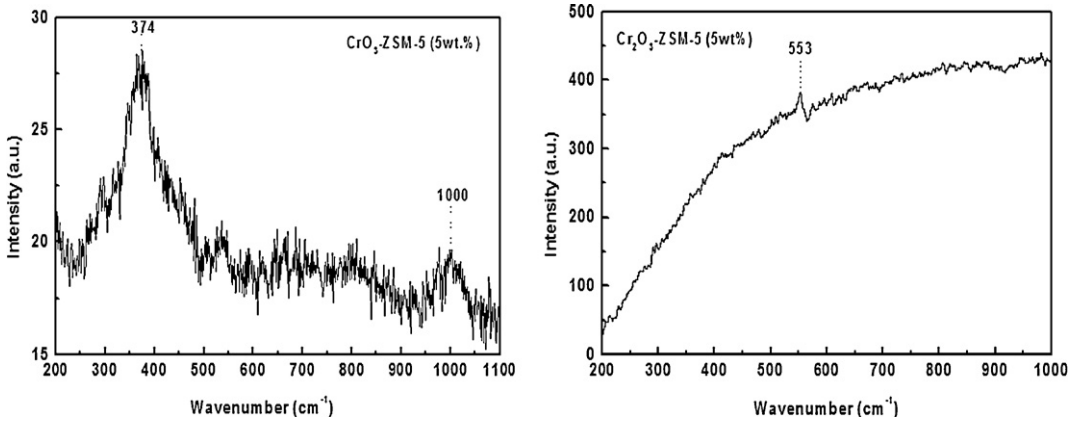

Fig. 7. Raman spectra of reference compounds.

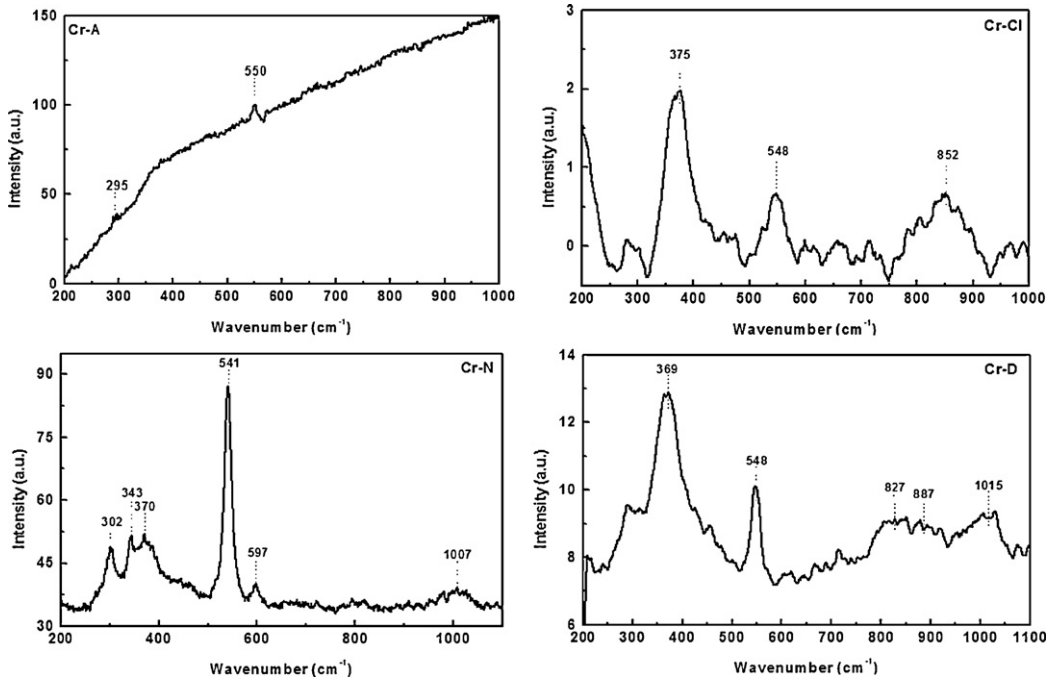

Fig. 8. Raman spectra of catalysts.

Table 4
XPS results.

	Cr–A	Cr–Cl	Cr–N	Cr–D
Surface atomic ratios				
Cr/Al	0.3	0.42	0.5	0.81
Si/Al	19.23	20	18.18	20.83
Cr/Si	0.016	0.021	0.028	0.039
Atomic surface concentration (%)				
Cr 2p	0.48	0.62	0.80	1.12
Si 2p	30.0	28.9	28.3	28.8
Al 2p	1.45	1.57	1.55	1.50
N 1s	0.25	0.41	0.38	0.36
C 1s	6.7	7.1	8.1	7.4
Bending energy (eV)				
Cr 2p 3/2	580.0	580.0	580.0	580.0
Cr 2p 3/2	576.3	576.9	576.9	576.5
Cr 2p 1/2	586.1	586.7	586.7	586.3
Cr 2p 1/2	589.8	589.8	589.8	589.8
Si 2p	103.8	103.8	103.8	103.8
Al 2p	75.4	75.3	75.3	75.3
Cr^{3+}/Cr^{6+} intensity ration (a.u.)				
	0.76	0.93	2.32	1.75

at 573–576.9 and 586.1–586.7 eV) [47,48]. In our study, it is difficult to ascertain the contribution of intermediate chromium states (Cr^{4+}, Cr^{5+}) in the Cr 2p3/2 region due to the intrinsic complexity of the Cr^{3+} component.

The Si/Al ratios of the external surface measured by XPS show that the catalysts surface is rich in silicon groups. The difference between the Si/Al ratios determined at surface by XPS and those determined in bulk by chemical analysis indicates an uneven distribution of silicon and aluminum throughout the zeolite structure. Cr/Al ratios are lower than the nominal value (Cr/Al = 1) because of the migration of metallic ions into the zeolite matrix during solid-state reaction.

Assuming the same relative response factor for Cr^{3+} and Cr^{6+} [49], the Cr^{3+}/Cr^{6+} intensity ratios can be calculated from XPS peak areas of both dominated chromium species (see Table 4). It seems that Cr–N and Cr–D catalysts contain highly dispersed Cr^{3+} oxide in an almost amorphous, microcrystalline or crystalline surface environment, as high fractions were detected by means of XPS and XRD in the case of Cr–N catalyst. In the case of Cr–A and Cr–Cl catalysts, 0.76 and 0.93 ratios indicate that a significant part of Cr^{6+} ions occupied exchange sites.

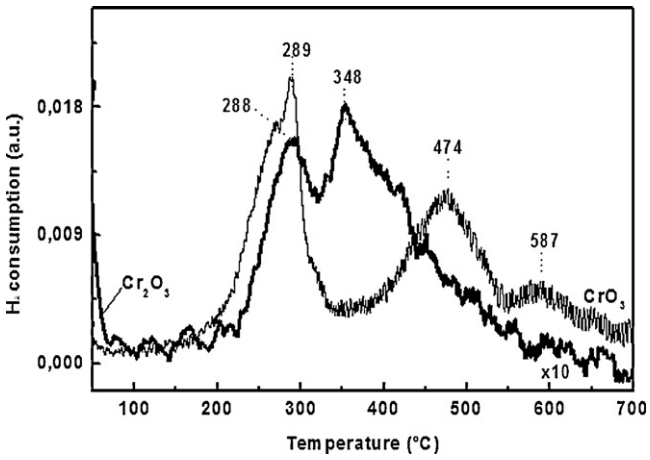

Fig. 9. H_2-TPR profile of chromium oxides.

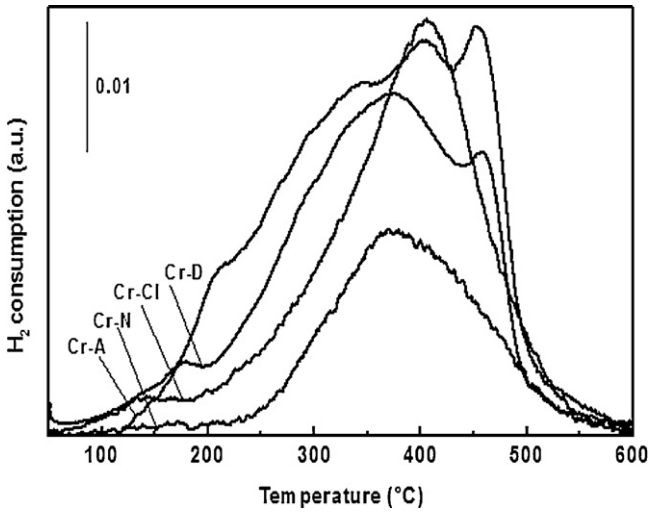

Fig. 10. H_2-TPR profiles of catalysts.

3.6. TPR

TPR profiles of reference oxides (CrO_3 and Cr_2O_3) and catalysts are shown in Figs. 9 and 10, respectively. Each catalyst profile was deconvoluted into Gaussian peaks in the order to determinate the maximal temperature of reduction. TPR results are compiled in Table 5.

Cr_2O_3 oxide exhibits two reduction peaks situated at 288 and 348 °C. The first peak is attributed to the reduction of Cr(VI) present on the surface of chromia [50], while the second corresponds to the reduction of Cr(III) to Cr(II) [50]. TPR profile of CrO_3 oxide shows three reduction peaks situated at 289, 474 and 587 °C, attributed to the reduction of Cr(VI) to Cr(III) [51–54].

The TPR profile of Cr–Cl catalyst shows a symmetric peak attributed to the reduction of Cr(VI) to Cr(III). According to the H_2/Cr ratio, the reduction of Cr^{6+} ions is total. These cations are probably located in the accessible sites of zeolite.

Cr–N catalyst exhibits two reduction peaks at 367, 451 °C. The first peak is attributed to the reduction of Cr(VI) present at the surface of the Cr_2O_3 oxide, while the second one (75% of total hydrogen consumption) is attributed to the reduction of Cr(III).

Cr–A and Cr–D catalysts exhibit broad TPR profiles evidencing the presence of both Cr(III) and Cr(VI) oxide species in the starting material.

H_2/Cr molar ratio values are lower than theoretical value required for a total reduction of Cr(VI) to Cr(III) according to $2CrO_3 + 3H_2 \rightarrow Cr_2O_3 + 3H_2O$.

In the case of Cr–A, Cr–D and Cr–N catalysts, H_2/Cr molar ratio values indicate that Cr(III) oxide hinders the reduction of Cr(VI). For Cr–Cl catalyst, the totality of Cr species is reduced since they are located at the exchange sites of the zeolite.

Table 5
TPR results.

Catalysts	H_2/Cr	T (°C)
Cr_2O_3	–	288, 348
CrO_3	1.5	289, 474, 587
Cr–A	0.26	219, 292, 358, 403, 454
Cr–Cl	1.6	137, 406
Cr–N	0.31	367, 451
Cr–D	0.48	168, 317, 408, 463

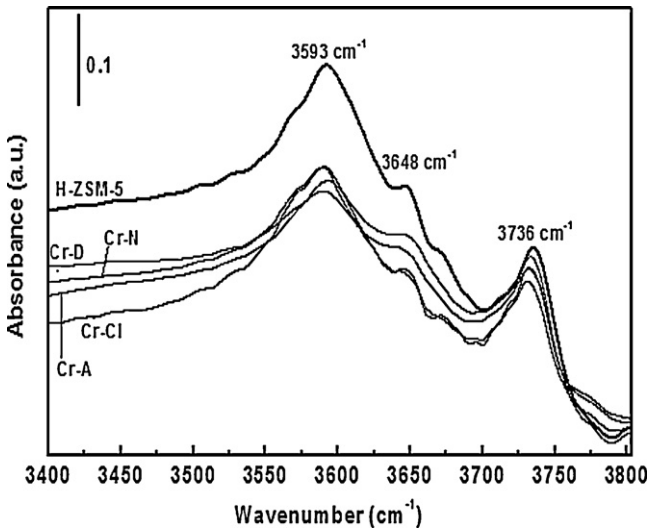

Fig. 11. DRIFT spectra of H–ZSM-5 and chromium containing catalysts.

3.7. DRIFT measurements

DRIFT spectra of Cr–ZSM-5 catalysts are reported in Fig. 11. Spectrum of H–ZSM-5 is also included as reference. It is seen that the intensity of the band at 3591 cm^{-1} assigned to the strong Brönsted acid sites Si–O^+H–Al [55,56] slightly decreases after chromium exchange. In contrast, the bands observed at 3647 and 3736 cm^{-1}, attributed to extra framework Al (Al–OH) [57,58] and terminal hydroxyl groups Si–OH [59,60], respectively, are always present in the spectra and do not undergo any significant change. This can indicates that extra-framework Al–OH and Si–OH do not participate significantly in the solid-exchange reaction but a part of Cr ions are probably exchanged on the strong Brönsted acid sites.

3.8. Catalytic activity

Catalytic performances in ethylene ammoxidation as a function of reaction temperature for the different catalysts are compiled in Table 6. Data were collected under stationary conditions after a stabilization period of 1 h. All catalysts are active and relatively selective towards acetonitrile. Wherein, Cr–Cl catalyst exhibits the highest ethylene conversion and the highest acetonitrile activity. There is no substantial difference between the Cr–A and Cr–D catalysts in terms of C_2H_4 conversion. However, high CO_2 selectivity was exhibited by the Cr–N catalyst (82% at 400 °C).

CrO_3 mechanically mixed with ZSM-5 is highly active and selective towards acetonitrile but Cr_2O_3–ZSM-5 is selective towards

Table 6
Ethylene ammoxidation results.

Catalyst	X (%)			S (%)			$A_{acetonitrile}$ ($\times 10^4$ mol g^{-1} h^{-1})		
	400[a]	450[a]	500[a]	400[a]	450[a]	500[a]	400[a]	450[a]	500[a]
Cr–A	3.65	11.28	15.85	77	89	92	0.57	2.62	3.53
Cr–Cl	3.12	13.87	26.15	37	89	95	0.24	2.84	6.49
Cr–N	4.67	6.71	11.50	16	56	89	0.16	0.87	2.57
Cr–D	4.22	12.30	17.30	70	93	94	0.67	2.87	4.98
CrO_3–ZSM-5	–	16.17	26.53	–	81	91	–	3.17	6.82
Cr_2O_3–ZSM-5	–	7.53	11.83	–	40	75	–	0.66	2.10

[a] Temp. (°C).

CO_2. This high activity of the CrO_3–ZSM-5 mechanical mixture is probably due solid state reaction between CrO_3 and H–ZSM-5 may proceed during the catalytic test since the Tamman temperature of CrO_3 is very low: ≈236 °C.

4. Discussion

Normally, the activity of a metal loaded zeolite is related to the level of metal exchanged. Nevertheless, the results of Table 6 show that Cr–Cl catalyst exhibits a superior performance taking into account C_2H_4 conversion and acetonitrile activity and selectivity. At lower temperatures, the low acetonitrile selectivity exhibited by Cr–Cl catalyst can be related to the presence of residual chloride ions. Furthermore, Cr–A catalyst is more active than Cr–N, although both catalysts contain almost the same amount of chromium but in terms of selectivity, Cr–N catalyst leads to a lower selectivity towards acetonitrile.

Cr–D catalyst exhibits a better activity and selectivity to acetonitrile than Cr–A and Cr–N, which are richer in chromium.

These diverse activity values seem to be related to the different chromium speciation obtained on the Cr–ZSM-5 catalysts. In the case of Cr–Cl and Cr–D catalysts, oxocationic Cr species seem to be the most active sites. On the other hand, the superiority of the catalytic behaviour of the Cr–Cl catalyst, which is poor in chromium, can be reinforced by the presence of chromium cations at the exchange sites, probably hydr(oxo) chromium cations, contrarily to Cr–D catalyst. In this latter sample, the excess of the chromium (ion exchange degree: 458%) seems to be loaded as oxide clusters which seem to be less active in ammoxidation.

Seeing that mono/poly-chromates ions are present in Cr–A and Cr–N catalysts, the low acetonitrile selectivity and activity obtained in the presence of Cr–N catalyst, leads to suggest that crystalline Cr_2O_3 inhibits the accessibility of active sites to the reactants.

In summary, chromium with high oxidation state (+VI) seems to play a key role in the ammoxidation reaction as confirmed by the catalytic behaviour of mechanical mixture of CrO_3 with ZSM-5. Furthermore, Cr(III) oxide seems to enhance the deep oxidation of the hydrocarbon.

5. Conclusion

Chromium can be highly dispersed in H–ZSM-5 matrix by solid-state ion exchange by choosing an appropriate chromium precursor. Spectroscopic analysis reveals that the higher oxidation state species were likely (poly)chromates (Cr(VI)), which are effective for the ammoxidation of ethylene. Indeed, the reduction of these Cr(VI) species into Cr^{3+} was demonstrated by TPR analysis. The exchange of chromium leads to the consumption of the Brönsted acid sites as shown by DRIFTS. The prepared materials exhibit generally good activity and selectivity in the studied reaction. Furthermore, an optimum of conversion was reached with the Cr–Cl catalyst, which is found to be the best catalyst towards the selective ammoxidation of ethylene into acetonitrile. This result can be explained by the best exchange level obtained when using $CrCl_3$(g) as the precursor, where, like for Fe–ZSM-5 system ($FeCl_3$ vaporisation), favours the presence of hydr(oxo) cationic species. It seems that the Cr(VI) species play a key role in the ammoxidation reaction, whereas the Cr_2O_3 oxide inhibits the catalyst activity.

References

[1] A.H. Tullo, Chem. Eng. News 87 (42) (2009) 9.
[2] Y. Li, J.N. Armor, J. Catal. 176 (1998) 495–502.
[3] R. Bulánek, K. Novoveská, B. Wichterlová, Appl. Catal. A: Gen. 235 (2002) 181–191.
[4] M. Mhamdi, S. Khaddar-Zine, A. Ghorbel, React. Kinet. Catal. Lett. 88 (2006) 149–156.
[5] F. Ayari, M. Mhamdi, G. Delahay, A. Ghorbel, J. Sol–Gel Sci. Technol. 49 (2) (2009) 170–179.
[6] J.-K. Wang, T. Komatsu, S. Namba, T. Yashima, T. Uematsu, J. Mol. Catal. 37 (1986) 327–338.
[7] B.D. Tagiev, K.M. Minachev, Uspekhi Khim 50 (1981) 1929–1959.
[8] E. Thursch, G. Szabo, J.M. Goupil, A. Chambellan, D. Cornet, J. Chem. Phys. 79 (1982) 479–487.
[9] B. Miedzinska, B.R. Hollebone, Can. J. Chem. 64 (1986) 1382–1389.
[10] F. Ayari, M. Mhamdi, G. Delahay, A. Ghorbel, Stud. Surf. Sci. Catal. 174B (2008) 1099–1102.
[11] M.R. Klotz, U.S. Pat. 4,299,808 (1981).
[12] E.M. Flanigen, B.M.T. Lok, R.L. Patton, S.T. Wilson, U.S. Pat. 4,759,919 (1988).
[13] B. Coughlan, W.A. McCann, W.M. Caroll, Chem. Ind. (1977) 358–360.
[14] J.R. Pearce, D. Sherwood, M.B. Hall, J.H. Lunsford, J. Phys. Chem. 84 (1980) 3215–3223.
[15] T. Yashima, J. Nagata, Y. Shimazaki, N. Hara, in: J.R. Katzer (Ed.), Molecular Sieves-II, American Chemical Society, Washington, 1977, pp. 626–634.
[16] A.V. Kucherov, A.A. Slinkin, Zeolites 7 (1987) 38–42.
[17] H.G. Karge, H.K. Beyer, Stud. Surf. Sci. Catal. 69 (1991) 43–46.
[18] A.V. Kucherov, A.A. Slinkin, J. Mol. Catal. 90 (1994) 323–354.
[19] S. Beran, P. Jiru, B. Wichterlovà, J. Chem. Soc., Faraday Trans. 79 (1983) 1585–1590.
[20] E.S. Shpiro, G.L. Tulecova, V.I. Zaikovskii, O.P. Tkachenko, T.V. Vasina, O.V. Bragin, K.K.M. Minachev, in: H.G. Karge, J. Weitkamp (Eds.), Zeolites as Catalysts, Sorbents and Detergent Builders, Elsevier, Amsterdam, 1989, pp. 399–408.
[21] J.R. Pearce, W.J. Mortier, J. Chem. Soc., Faraday Trans. 77 (1981) 1935–1944.
[22] R.S. Da Cruz, A.J.S. Mascarenhas, H.M.C. Andrade, Appl. Catal. B 18 (1998) 223–231.
[23] J.S. Olgen, R.S. Wyatt, J. Chem. Soc., Dalton Trans. 4 (1987) 859–865.
[24] G. Delahay, D. Valade, A.G. Vargas, B. Coq, Appl. Catal. B: Environ. 55 (2005) 149–155.
[25] J.H. DeBoer, B.C. Lippens, J. Catal. 3 (1946) 38–43.
[26] F. Schüth, R. Althoff, J. Catal. 143 (1993) 388–394.
[27] K.F.M.G.J. Scholle, W.S. Veeman, P. Frenken, G.P.M. Van de Velden, Appl. Catal. 17 (1985) 233–259.
[28] J.C. Jansen, F.J. Van der Gaag, H. Van Bekken, Zeolites (1984) 369–372.
[29] E.M. Flaningen, H. Khatami, H.A. Szymanski, Adv. Chem. Ser. 101 (1971) 201–229.
[30] C.A. Fyfe, Y. Feng, H. Grondey, G.T. Kokotailo, H. Gies, Chem. Rev. 91 (1991) 1525–1543.
[31] B.M. Weckhuysen, H.J. Spooren, R.A. Schoonheydt, Zeolites 14 (1994) 450–457.
[32] B.M. Weckhuysen, L.M. De Ridder, R.A. Schoonheydt, J. Phys. Chem. 97 (1993) 4756–4763.
[33] B.M. Weckhuysen, A.A. Verberckmoes, A.L. Buttiens, R.A. Schoonheydt, J. Phys. Chem. 98 (1994) 579–584.
[34] B.M. Weckhuysen, P. Vand Der Voort, G. Catana, Spectroscopy of Transition Metal Ions on Surface, Leuven University Press, 2000, p. 243.
[35] B.M. Weckhuysen, I.E. Wachs, R. Schoonheydt, Chem. Rev. 96 (1996) 3327–3349.
[36] F.D. Hardcastle, I.E. Wachs, J. Mol. Catal. 46 (1988) 173–186.
[37] D.H. Cho, S.D. Yim, G.H. Cha, J.S. Lee, Y.G. Kim, J.S. Chung, I.-S. Nam, J. Phys. Chem. A 102 (1998) 7913–7918.

[38] S.D. Yim, D.J. Koh, I.-S. Nam, Y.G. Kim, Catal. Lett. 64 (2000) 201–207.
[39] M.A. Vuurman, D.J. Stufkens, A. Oskam, J.A. Moulijn, F. Kapteijn, J. Mol. Catal. 60 (1990) 83–98.
[40] M.A. Vuurman, I.E. Wachs, J. Phys. Chem. 96 (1992) 5008–5016.
[41] H.H. Kung, Adv. Catal. 40 (1994) 1–38.
[42] G. Deo, I.E. Wachs, J. Phys. Chem. 95 (1991) 5889–5895.
[43] M.A. Vuurman, I.E. Wachs, D.J. Stufkens, A. Oskam, J. Mol. Catal. 80 (1993) 209–227.
[44] M.A. Vuurman, F.D. Hardcastle, I.E. Wachs, J. Mol. Catal. 84 (1993) 193–295.
[45] M. Cherian, M.S. Rao, A.M. Hirt, I.E. Wachs, G. Deo, J. Catal. 211 (2002) 482–495.
[46] L. Zhang, Y. Zhao, H. Dai, H. He, C.T. Au, Catal. Today 131 (2008) 42–54.
[47] F. Simard, U.A. Sedran, J. Sepŭ1veda, N.S. Fîgoli, H.I. de Lasa, Appl. Catal. A: Gen. 125 (1995) 81–98.
[48] NIST X-ray Photoelectron Spectroscopy Database, NIST Standard Reference Database 20, Version 3.5.
[49] J.H. Scofield, J. Electron. Spectrosc. 8 (1976) 129–137.
[50] L.I. Ilieva, D.H. Andreeva, Thermochim. Acta 265 (1995) 223–231.
[51] W.K. Jóźwiak, W. Ignaczak, D. Dominiac, T.P. Maniecki, App. Catal. A: Gen. 258 (2004) 33–45.
[52] B.L. Chamberland, Solid State Mater. Sci. 7 (1977) 1–31.
[53] T.A. Hewston, B.L. Chamberland, J. Magnet. Mater. 43 (1984) 89–95.
[54] N.E. Fouad, J. Therm. Anal. 31 (1986) 825–834.
[55] J. Ward, J. Catal. 9 (1967) 225–236.
[56] A.W. Chesr, R.M. Dessarn, L.B. Alemani, G.J. Woolevy, Zeolites 6 (1986) 14–16.
[57] E. Loffler, U. Lohse, Ch. Penker, G. Oehmann, L.M. Kustov, V.L. Zholobenko, V.B. Kazansky, Zeolites 10 (1990) 266–271.
[58] E. Gallei, D. Eisenbach, J. Catal. 37 (1975) 474–485.
[59] U. Lhose, E. Löffler, M. Hunger, J. Stöckner, V. Patzelove, Zeolites 7 (1987) 11–13.
[60] A. Jentys, G. Rumplmayr, J.A. Lercher, J. Appl. Catal. 53 (1989) 299–312.